Saddle point for oxygen reorientation in the vicinity of a silicon vacancy

L. Dobaczewski,[1,2,3,*] O. Andersen,[2] L. Rubaldo,[2,4] K. Gościński,[1] V. P. Markevich,[2] A. R. Peaker,[2] and K. Bonde Nielsen[3]

[1]*Institute of Physics, Polish Academy of Sciences, al. Lotnikóy 32/46, 02-668 Warsaw, Poland*

[2]*Centre for Electronic Materials, Devices and Nanostructues, University of Manchester Institute of Science and Technology, P. O. Box 88, Manchester M60 1QD, United Kingdom*

[3]*Institute of Physics and Astronomy, University of Aarhus, Ny Munkegade, DK-8000 Aarhus C, Denmark*

[4]*CNRS/MPI, High Magnetic Field Lab, 25 ave des Martyrs, BP 166, 38046 Grenoble, France*

(Received 1 November 2002; published 22 May 2003)

A piezospectroscopic analysis of the vacancy-oxygen complex in silicon has enabled us to demonstrate that this defect in the unstable configuration of the saddle point on the reconfiguration trajectory has a trigonal symmetry. This unstable defect configuration may be considered as the precursor for an oxygen diffusion process where the migrating oxygen atom is accompanied by a vacancy. The trigonal saddle point configuration results in a strong electrical polarization of the pair which can aid the jumping to a neighboring unit cell. This scenario is very plausible to explain how vacancies can drag oxygen atoms through the crystal to form larger oxygen aggregates.

I. INTRODUCTION

Silicon crystals grown by the Czochralski method contain approximately 10^{18} cm^{-3} atoms of oxygen. This oxygen affects the electrical and mechanical properties of the crystals very significantly. During thermal processing the oxygen may aggregate forming a family of defects known as thermal donors.[1] The microscopic processes leading to oxygen aggregation are still debated, as the energy barrier for the process is much smaller than the barrier for the hopping of an isolated interstitial oxygen atom. This means that oxygen diffuses as a part of a defect complex. There is evidence indicating that this complex is an oxygen dimer.[2,3] However, there is also the possibility that the vacancy-oxygen (VO) complex could be an alternative oxygen aggregation vehicle, in particular, when vacancies are able to trap oxygen atoms effectively.[4-8] Further thermal processing of samples containing VO complexes leads to a gradual appearance of VO$_2$ complexes resulting from the diffusing VO pairs being trapped by the interstitial oxygen atoms.[7,9-11] Eventually, larger oxygen aggregations may form assisted by vacancies.

Lattice thermal vibrations result in the defect complexes reconfiguring within the unit cell of the crystal. We showed recently that in some cases this reconfiguration sets in at temperatures similar to, or slightly lower than the temperatures at which long-range diffusion or dissociation of the defect occurs.[12] Consequently, in such cases the defect reconfiguration may be considered a precursor to diffusion because the microscopic mechanism of both processes is similar. In order to take up an alternative equivalent position in the crystal unit cell a defect complex has to overcome an energy barrier. Usually very little is known about the structure of this barrier because although the reconfiguration trajectory of a defect can be modeled, it is extremely difficult to confirm this trajectory experimentally. However, the barrier for the reconfiguration process can be measured and represents the energy difference between the stable defect configuration and the saddle point of the reconfiguration trajectory.

For the case of the interstitial oxygen in silicon different reorientation scenarios have been proposed to explain a barrier of 2.5 eV for a single oxygen jump between neighboring bridging positions.[13] Basically, either adiabatic processes, where during the reconfiguration of oxygen all surrounding atoms are fully relaxed, or nonadiabatic ones allowing for dynamic effects, were considered. In the former case a defect in the saddle point should have a meaningful (high-symmetry) configuration, whereas in the latter case the saddle point looses its meaning to the extent that it results from averaging over momentarily nonequilibrium distributions of atoms. The difference between these two approaches is basically a question of the degree of departure of moving atoms from adiabatic trajectories during the reorientation process. Thus keeping this averaging in mind the application of the adiabatic approach still allows some temporary atom displacements. Similar averaged atom positions are considered when a fixed orthorhombic atom symmetry of VO is concluded from the piezospectroscopic analysis of the experimental data. See, e.g., Refs. 14 and 15 for a discussion of the interstitial oxygen reconfiguration trajectory in silicon and consequences of the adiabatic versus nonadiabatic approach to the defect reorientation process.

The vacancy-oxygen pair is the main radiation defect in oxygen-rich crystals but can also be generated during the Czochralski growth process.[16] The stable microscopic structure of the complex has been determined by Watkins and Corbett[17] and confirmed by theoretical modeling.[18-23] It is now well-established experimentally that VO has orthorhombic C_{2v} symmetry (Fig. 1) and when the defect is in the neutral charge state the effective barrier for reconfiguration of the oxygen atom is 0.38 eV.[17,25] This barrier has also been calculated and found to be equal to 0.47,[18] 0.5,[19] 0.3,[20] and 0.26 eV.[21] In the first of these references it was concluded that saddle point for oxygen reconfiguration is in the $\langle 110 \rangle$ (Ref. 26) direction from the substitutional site, whereas in the next three references it has been postulated that the saddle point configuration has trigonal symmetry. Pesola *et al.*[20] further found an alternative saddle point of T_d symme-
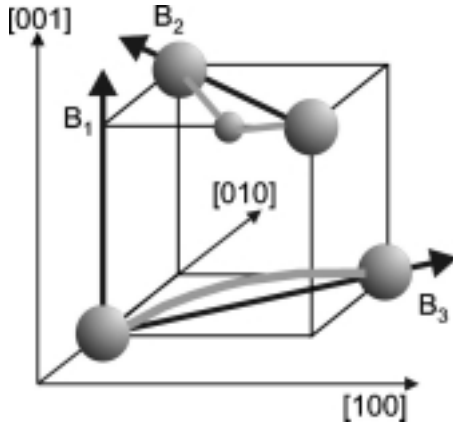
FIG. 1. The structure of the VO complex after Ref. 17. The arrows indicate principal axes of Kaplyanskii's (Ref. 24) piezospectroscopic tensor for orthorhombic-I symmetry. The labels B_1, B_2, and B_3 denote the corresponding eigenvalues.

try (substitutional position of oxygen) 0.6 eV above the equilibrium configuration.

In this article we report an extensive piezospectroscopic analysis of the vacancy-oxygen complex in silicon and demonstrate (in the framework of an adiabatic treatment) that the defect has trigonal symmetry in the unstable configuration of the saddle point. We further suggest that the saddle point configuration of VO can be considered to be the first step in an oxygen diffusion process assisted by vacancies.

II. EXPERIMENTAL RESULTS

We have applied high-resolution deep level transient spectroscopy [Laplace DLTS (Ref. 27)] combined with uniaxial stress to obtain a complete description of how the total energy of the vacancy-oxygen pair in the neutral or negative charge states responds to stress. We used samples cut from Czochralski n-type 20 Ω cm silicon shaped as $1 \times 2 \times 7$ mm stress bars. A series of samples were cut from the same (110) wafer with the longest sample edge along $\langle 100 \rangle$, $\langle 110 \rangle$, or $\langle 111 \rangle$, respectively. All samples were furnished with evaporated Au Schottky diodes. The VO pairs were produced by either proton implantation with an energy of 525 keV and a dose of $\sim 5 \times 10^9$ cm^{-2} or electron irradiation with an energy of 2 MeV and a dose of $\sim 6 \times 10^{13}$ cm^{-2}.

Results from three different types of experiments have been obtained and form the basis of our analysis. (a) Splitting of Laplace DLTS emission peaks: this kind of measurements records the influence of stress on the ionization process $VO^- \rightarrow VO^0 + e_c^-$ and contains information that depends on both charge states of the defect simultaneously. (b) Stress induced alignment: here the total energy shifts for different orientations of the defect resulting from alignment under stress for the VO^- and VO^0 charge states are obtained. This type of measurement provides information on the strain tensor for individual charge states. (c) Defect reorientation kinetics: these measurements provide the stress-induced changes in the defect reorientation barriers which relate to saddle-point symmetry.

For a defect of given symmetry the response to the stress

can be described within the piezospectroscopic theory, in which the stress potential energy may be expressed as $\Delta E = \Sigma B_{ij} \varepsilon_{ij}$, where ε_{ij} are components of the strain tensor and B_{ij} are components of the corresponding piezospectroscopic tensor.[24,28] Symmetry considerations allow us to choose the defect characteristic reference system (Fig. 1) in which the piezospectroscopic **B** tensor is diagonal and then calculate the energy shifts from Tr($\mathbf{B}\varepsilon$) with the silicon strain tensor ε transformed from its standard cubic-axes reference system to the principal system of **B**.

The reconstructed Si-Si bond (along the $\langle 110 \rangle$ direction in Fig. 1) can have six equivalent orientations in the unit cell. The stress applied along one of the principal axes of silicon partially lifts this sixfold spatial degeneracy and shifts the defect total energy differently for, what are now, nonequivalent defect orientations. For the $\langle 100 \rangle$ stress direction four configurations of the reconstructed bond are affected by the stress in the same way and different from the other two (see Ref. 17 for details of the piezospectroscopic analysis). The total energies of these two groups of configurations separate with the stress coefficient

$$\alpha_{\langle 100 \rangle} = \tfrac{1}{2}(s_{11} - s_{12})[(B_2 - B_3) - 2(B_2 - B_1)], \qquad (1)$$

where the components for the silicon elastic compliance tensor are $s_{11} = 7.68 \times 10^{-3}$ GPa^{-1} and $s_{12} = -2.14 \times 10^{-3}$ GPa^{-1}. For the $\langle 110 \rangle$ stress direction there are three groups of the reconstructed bond configurations so one can have two different stress coefficients

$$\alpha'_{\langle 110 \rangle} = \tfrac{1}{4}(s_{11} - s_{12})[(B_2 - B_3) - 2(B_2 - B_1)] + \tfrac{1}{4}s_{44}(B_2 - B_3) \tag{2}$$

for the Si-Si bond oriented along [110] with $s_{44} = 12.6 \times 10^{-3}$ GPa^{-1} and, e.g., [011] direction, and

$$\alpha''_{\langle 110 \rangle} = \tfrac{1}{2}s_{44}(B_2 - B_3) \tag{3}$$

for the Si-Si bond oriented along [110] and [$\bar{1}$10] directions. Finally, for the $\langle 111 \rangle$ stress direction there are two equal groups of configurations separating with the stress coefficient

$$\alpha_{\langle 111 \rangle} = \tfrac{1}{3}s_{44}(B_2 - B_3). \tag{4}$$

A. Laplace DLTS peak splitting

In this experiment the samples were kept at constant temperature and the influence of stress on the Laplace DLTS spectra was observed. Figure 2 shows the effect of the stress on the Laplace DLTS peak. The pattern of split peaks agrees with the orthorhombic defect symmetry as found by Watkins and Corbett[17] with the use of magnetic resonance techniques. For the $\langle 100 \rangle$ stress direction the Laplace DLTS peak of VO splits in to two peaks with the amplitude ratio 2:4. For the $\langle 110 \rangle$ stress direction the energy level of an orthorhombic defect should split with amplitudes in the ratios 1:4:1, however, in this case the first two lines at low stress are not resolved, thus only two peaks with a 5:1 amplitude ratio are observed. Finally, for the $\langle 111 \rangle$ stress direction the peak splits into two equally intense peaks (3:3).
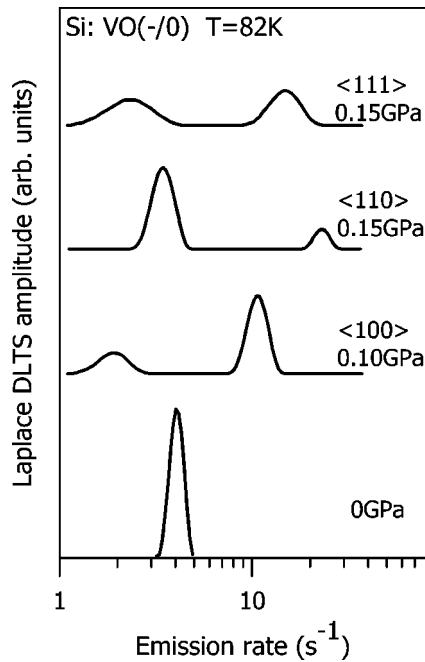
FIG. 2. Laplace DLTS spectra for the VO complex taken without stress and with stress applied along three major crystallographic directions. The amplitudes of the stress-split peaks sum up to the value observed without the stress. Note the small stress values needed to observe the Laplace DLTS peak splitting.

A similar pattern of splitting has been observed also with a use of the conventional DLTS method with a much lower energy resolution.[25,29] In our experience a use of the conventional DLTS temperature-scan technique combined with the uniaxial stress complicates data interpretations in the present case due to a fact that VO begins to reorient at temperatures only slightly higher than those where the DLTS signal is observed, which means the shape of a partly resolved stress-split signal may be affected.

Figure 3 shows the stress-induced Laplace DLTS peak shifts. The frequency scale of the emission spectra has been converted to an energy scale of the splitting assuming that the pre-exponential factor of the emission formula[30] is unaffected by the stress. All peak positions converge towards the zero-stress value and move linearly with the stress with the exception of the low-frequency $\langle 100 \rangle$ branch, which reveals a very clear and reproducible stress nonlinearity.

B. Alignment of VO in neutral and negative charge states

In the alignment experiment the stress is applied to the sample at a relatively high temperature to assure that the equilibrium distribution between the nonequivalent defect orientations is reached. Then the sample is quickly cooled to the measurement temperature (around 90 K), at which the Laplace DLTS spectra are recorded in order to evaluate how the populations of the nonequivalent defect orientations deviate from their random values for a given defect symmetry. Assuming that this configuration redistribution is governed by Boltzman statistics at the alignment temperature the total energy separation of nonequivalent configurations can be de-
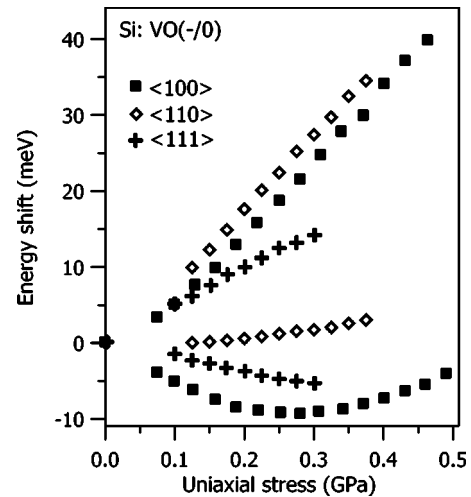

FIG. 3. Stress-induced Laplace DLTS peak shifts for the stress oriented along three major crystallographic directions. The energy shift is assumed to be proportional to the term $kT \times \ln[e_n(P)/e_n(P=0)]$, where e_n is the peak frequency at a given stress P and T is the measurement temperature.

duced and information on the piezospectroscopic tensor obtained from the Eqs. (1)–(4). Because the defect is embedded in the space charge region of a Schottky diode its charge state can be controlled during the alignment process by varying the sample bias. Hence, one can assure that the VO defect species are all in the neutral charge state (the sample is reverse biased) or all in the negative charge state (the bias is off). We find that VO reorients much slower in its negative charge state than in its neutral charge state. As a result, alignment experiments are easily performed for the latter case as removal of the bias practically stops the alignment. Hence, bias removal after aligning under reverse bias allow us to cool the sample with frozen-in aligned populations of the nonequivalent spatial orientations of the VO center. For the negative charge state the alignment process is so slow that it is difficult to achieve full alignment at an allowed temperature, i.e., one at which the Fermi level is above the VO level. Furthermore, no freeze-in is possible. Consequently, some change in the alignment could occur during cooling; either alignment recovery or further alignment depending on reorientation barrier heights for the various stress orientations. Hence, despite the special care taken to align for sufficient long period of time and cool as fast as possible we may not have avoided completely that the alignment data obtained for the negative charge state could include some systematic errors.

Figure 4 shows an example of the alignment effect observed on the Laplace DLTS spectra taken for $\langle 110 \rangle$ stress. For this stress direction the initial splitting pattern with amplitudes in the ratios 1:4:1 (here observed as 5:1) converts after the complete alignment process (dashed line) to the 3:0:3 pattern (here observed as 3:3). For the $\langle 100 \rangle$ stress direction the Laplace DLTS peak initial splitting 2:4 after the alignment changes to 0:6, while for the $\langle 111 \rangle$ direction the initial splitting is 3:3 with no alignment effect in the neutral charge state. The measured stress coefficients obtained by alignment for both charge states and all three stress direc-
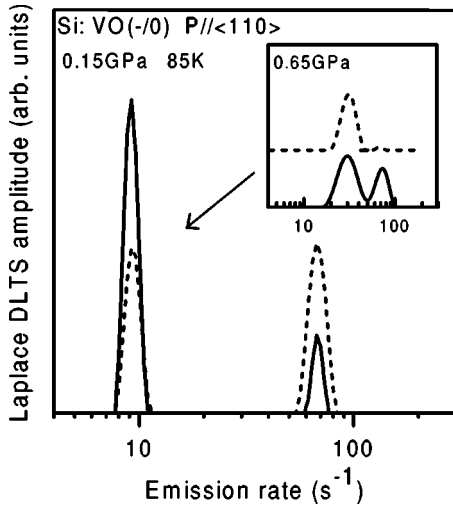
FIG. 4. Laplace DLTS spectra taken for the VO complex in the $\langle 110 \rangle$ stress direction before (solid line) and after (dashed line) complete defect alignment. The inset shows the splitting of the left-hand side peak at a much larger stress.

tions are summarized in Table I, which also includes the coefficients obtained from Laplace DLTS peak splitting. Note that for the $\langle 100 \rangle$ stress direction the bending effect is indicated by including both a low- and high-stress splitting coefficient. Due to the fact that the stress-induced shifts of the Laplace DLTS peaks reflect the influence of the stress on the defect ionization process $VO^- \rightarrow VO^0 + e_c^-$ the values given in Table I for VO^0 and splitting should, in principle, sum up in a row to the value for VO^- where the influence of the stress on the band gap cancels out. Keeping in mind possible systematic errors for α^- the values for the $\langle 110 \rangle$ and $\langle 111 \rangle$ stress directions agree satisfactorily. For the $\langle 100 \rangle$ stress direction it is obvious that the high-stress asymptotic value of the splitting coefficient fits better to the measured values of $\alpha^0_{\langle 100 \rangle}$ and $\alpha^-_{\langle 100 \rangle}$. Below we discuss how this may be understood in terms of a contribution from stress dependence of the capture cross section.

For a defect with the orthorhombic symmetry there are seven nonequivalent stress orientations. The low-frequency branch, which in Fig. 3 reveals the nonlinearity, corresponds to the stress applied along the [001] direction. This particular stress orientation has two unique features. First, for this stress direction the crystal of silicon experiences considerable tensile strain along the [110] direction, i.e., along the

TABLE I. Values (in meV/GPa) of the alignment stress coefficients α for VO in both charge states and the Laplace DLTS peak splitting. Note that signs of the peak splitting coefficients have been chosen so they correspond to the assumed level sequence in the alignment experiment.

Stress direction	VO^0	Splitting	VO^-
$\langle 100 \rangle$	151	$-140 \rightarrow -56$	120
$\langle 110 \rangle$	93	-78	0
$\langle 111 \rangle$	0	64	42

Si-Si bond of the VO complex. Second, the compressive strain along [001] is larger than for any other stress orientation. This piezoscopic uniqueness is likely to be the reason why significant nonlinearity is found only for the [001] branch of the stress split pattern of Fig. 3. Our direct measurements of the capture process for individual stress-split components showed that there is a very strong initial decrease of the electron capture cross section for the [001] branch. A similar effect has been reported previously for this particular branch.[29,31] The pronounced stress dependence of the capture rate for the [001] branch is in contrast in to the case of $\langle 111 \rangle$ stress where we found the capture rate to be almost independent of stress. The dramatic decrease in [001] capture rate can be explained only in terms of a stress-induced modification of the relaxation associated with the emission process. We believe that the same relaxation is likely to be responsible for the observed nonlinearity and thereby for the lack of correspondence between the low-stress splitting and the alignment data for the $\langle 100 \rangle$ stress directions.

To pursue this idea further we notice that a hydrostatic pressure study of the VO defect has shown that a substantial decrease in the defect volume can be associated with the electron emission process.[32] This complies with a significant relative lattice relaxation being associated with the two charge states involved in the VO emission at zero stress. This relaxation, however, does not result in an electron-capture barrier measurable by standard methods.[33] The Henry and Lang semiclassical model[34] treats the relaxation and links the electron-phonon coupling with a phenomenological energy barrier of the carrier capture process which obviously is included in our measured activation energies. In order to explain our results we may then assume that the capture is stress dependent. It is gratifying then that the measured stress dependence of the capture barrier complies quantitatively with the bending of the [001] branch.

Finally, we note that Watkins and Corbett[17] measured the stress-induced electron redistribution process at low stress and that this measurement is equivalent to the Laplace DLTS peak splitting measurement provided the stress does not affect the capture process. The redistribution process is governed by steady state occupancies of different defect configurations and thus any changes in the capture processes are not in the redistribution effect observed. We have noticed that at high stress the capture rate of the low-frequency branch becomes independent of stress and that the high-frequency branch exhibits only a slight increase. Consequently, the Laplace DLTS splitting value observed at high stress should approach the value obtained by Watkins and Corbett at low stress from the redistribution process analysis. We conclude that the splitting and alignment data are fully consistent when the stress dependence of the capture process is taken into account.

The alignment data experiment allows us to obtain the following relations for the components of the piezospectroscopic tensor as defined in Fig. 1. For the neutral charge state (denoted by the superscript 0) we obtain $B_2^0 = B_3^0$ [from the value of $\alpha^0_{\langle 111 \rangle}$ and Eq. (4)] and $B_2^0 - B_1^0 = 17$ eV [from the averaged values obtained from $\alpha^0_{\langle 100 \rangle}$ with Eq. (1) and $\alpha'^0_{\langle 110 \rangle}$

TABLE II. Values (in eV) of the piezospectroscopic tensor components for VO in both charge states assuming that $B_1+B_2+B_3=0$.

Tensor component	Theory [a]	EPR [b]	Laplace DLTS [c]
B_1^0	−9.8	−11.1	−11.4
B_2^0	5.5	6.1	5.7
B_3^0	4.5	4.9	5.7
B_1^-	−6.8	−8.4	−8.0
B_2^-	7.8	8.8	9.0
B_3^-	−0.5	−0.4	−1.0

[a]Reference 21.
[b]Reference 35.
[c]This work.

with Eq. (2)]. Note that all αs have been measured for the compressive (negative) stress thus for the calculations their opposite signs have to be used. For the negative charge state we obtained $B_2^- - B_3^- = 10$ eV [$\alpha_{\langle 111 \rangle}^-$ and Eq. (4)] and $B_2^- - B_1^- = 17$ eV [$\alpha_{\langle 100 \rangle}^-$ and Eq. (1)] with a typical error of 0.5 eV for all values. When the constraint of a traceless piezospectroscopic tensor ($B_1+B_2+B_3=0$) is imposed then the values of the tensor components for both charge states are consistent with those obtained by the magnetic resonance measurements (EPR) and theoretical modeling (see Table II).

C. Stress-induced variations of the reorientation barrier

In the third type of the experiment the influence of the stress on the defect reorientation barrier has been measured. The alignment process was examined in a sequence of isothermal annealing steps. After each step the concentrations of the nonequivalent configurations were obtained. This experiment enables the reorientation kinetics to be quantified, and, as a result, the stress coefficient of the reorientation barrier can be calculated. The experimental data were recorded for both the neutral and negative charge states of the VO complex. Figure 5 shows the reorientation kinetics for the neutral charge state for the $\langle 100 \rangle$ [Fig. 5(a)] and $\langle 110 \rangle$ [Fig. 5(b)] stress directions. In the first case the stress speeds up the reorientation process in contrast to the latter case where the effect of stress on the process is opposite. We derive from the data that the stress in the $\langle 100 \rangle$ direction lowers the barrier with a stress coefficient of -84 ± 8 meV/GPa, while for the $\langle 110 \rangle$ stress the barrier increases with a coefficient 100 ± 3 meV/GPa. For the zero-stress barrier for VO^0 we get the value 388 meV close to the figures obtained previously.[17,25] The barrier for VO$^-$ cannot be measured by analyzing the reorientation kinetics in the negative charge state. We find that this barrier is so large that it is much faster for the defect to reconfigure by losing an electron and reorient in the resultant neutral charge state.

III. DISCUSSION AND CONCLUSIONS

A. Saddle point symmetries for adiabatic reorientation process

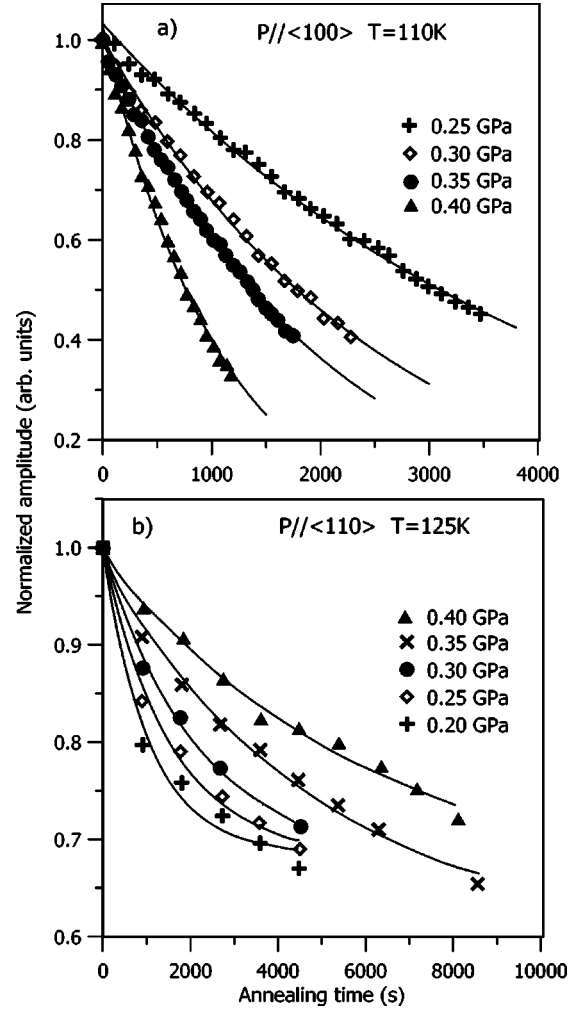In practice, there are four high-symmetry cases of a possible saddle point configuration.

FIG. 5. The VO^0 reorientation kinetics measured as a decrease or increase of amplitude of one of the stress-split Laplace DLTS peaks (e.g., a gradual transformation of the solid line spectrum in Fig. 4 to the dashed line one as a result of a series of the isochronal annealings at a given temperature). For the $\langle 100 \rangle$ direction (a) the reorientation time constants are 73, 44, 33, 18 mins for the stress equal 0.25, 0.30, 0.35, and 0.40 GPa, respectively, while for the $\langle 110 \rangle$ direction (b) the reorientation time constants increase with the stress and equal: 17, 26, 39, 60, and 111 min for the stress 0.20, 0.25, 0.30, 0.35, and 0.40 GPa, respectively.

(a) Cubic when the oxygen atom in the saddle point configuration is in the substitutional position of T_d symmetry. The total energy of this configuration can not be split by the application of uniaxial stress along any crystallographic direction. Consequently, the difference in the barrier stress coefficients should be solely due to different stress responses of the defect stable configuration (the bottom of the barrier) for different stress orientations. With the measured values of the piezospectroscopic tensor (assumed to be traceless), the bottom of the barrier shifts upwards by 110 and 29 meV/GPa for the stress orientation along the $\langle 100 \rangle$ and $\langle 110 \rangle$, respectively. These values cannot be rescaled by any shift (the same for both cases) of the barrier top to explain the observed values (-84 and 100 meV/GPa, respectively). A similar conclusion is reached even if a realistic finite trace is

allowed for, and, consequently, we can reject a possibility that the saddle point configuration has a cubic symmetry.

(b) Orthorhombic when the oxygen atom shifts along the C_{2v} axis on the (110) plane, but not as far as the substitutional point. In this reorientation scenario, the Si-O-Si bridge is stretched along the C_{2v} axis until oxygen reaches the saddle point where it detaches from one Si atom, swings towards a neighboring silicon and forms another stretched Si-O-Si bridge which then subsequently relaxes in the new symmetry plane. In this case the symmetry of the stable and saddle point configurations is the same, thus each stable configuration has its own saddle point for the reconfiguration process. Consequently, when the defect reconfigures from one configuration to another it always has to pass two saddle points.[36] In general, the effect of uniaxial stress on the energy of a point of a given symmetry results from a combination of the hydrostatic and the traceless components of the stress tensor. The traceless components shift the tops of the nonequivalent barriers in opposite directions around a hydrostatic shift. Consequently, with a realistic hydrostatic component (of any sign) the effective reorientation barrier of the orthorhombic symmetry should increase for any direction of the applied stress, because the larger one of two barriers will always be measured. Obviously, this is in contradiction to the decrease of the barrier observed for the $\langle 100 \rangle$ stress direction.

(c) Trigonal when oxygen is attached to three silicon atoms and is situated on the C_{3v} trigonal axis. In this case when during reorientation the Si-O-Si bridge stretches two electrons from the elongated Si-Si bond attach to oxygen forming a threefold coordinated structure of the saddle point. Then one of the initial Si-O bonds eventually breaks and a new elongated Si-Si bond forms. For this trigonal saddle point symmetry and stress orientation along the $\langle 100 \rangle$ direction the top of the barrier should shift the same way for all three equivalent $\langle 100 \rangle$ stress directions. In contrast to this, two different values of the saddle point total energy are envisaged for the $\langle 110 \rangle$ direction. This would result in two different energy barriers for the defect reorientation with different stress dependencies.

(d) Monoclinic when oxygen moves between the initial and final configurations following the shortest trajectory. Then the saddle point can be halfway, i.e., somewhere on a (110) symmetry plane between these two positions. It has been observed that for the $\langle 110 \rangle$ stress direction the alignment experiments lead to conversion of the 1:4:1 splitting pattern to the 3:0:3 one. It can be shown that if the saddle point configuration has a monoclinic symmetry then for this stress direction there are two nonequivalent paths for the reorientation from the fourfold degenerated configuration to a nondegenerated one and there are similar two paths for the reorientation to the other nondegenerated configuration as well. On each of the paths there is a different energy barrier of the saddle point. As a result, during the alignment process the defect having two different barriers for the reconfiguration chooses the lower one and this barrier would be the same for the reconfiguration from the fourfold degenerated configuration to any of the nondegenerated ones. For the case (b) we have concluded that on the defect reorientation

trajectory oxygen could have two barriers to overcome one by one and thus the effective barrier would have to increase with stress. In this case we have two alternative barriers thus the effective barrier should decrease and this decrease has to be the same for reconfiguration to any of the nondegenerated orientations. This conclusion is in conflict with our observations where for this stress directions it has been found that the barrier increases with stress.

Of the above four cases of possible saddle point symmetry (a)–(d) only the assumption of a trigonal saddle point (c) allows us to interpret the observed stress-induced shifts of the VO stable configurations and measured changes in the reorientation barriers in a consistent way for all stress directions.

B. Analysis of the reorientation process

We emphasize that our analysis in this section to determine the saddle point symmetry is based entirely on alignment and reorientation data obtained for the *neutral* charge state. Hence, the conclusions reached are independent of both peak splitting data and alignment data for the negative-charge state. The piezospectroscopic analysis of these data has been included primarily to show the consistency of the present work with previous results.

In the case of trigonal symmetry the **B** tensor can be decomposed in a hydrostatic component B_h and traceless components that depend on only one parameter. This parameter B_t can be obtained directly and independent of B_h from measured stress-energy splits. For trigonal saddle-point symmetry and for the $\langle 100 \rangle$ stress direction the total energy of the barrier top should shift only by the hydrostatic term $B_h(s_{11} + 2s_{12})$, whereas for the $\langle 110 \rangle$ stress direction the saddle point energy should split into two components according to the stress term $B_h(s_{11} + 2s_{12}) \pm B_t s_{44}/2$.

In Fig. 6 we document and visualize the trigonal symmetry of the saddle point through the construction of a total energy diagram for the VO pair stressed along the $\langle 110 \rangle$ direction. For this stress direction there are three different orientations of the Si-Si bond with respect to the stress, and these orientations are represented by three minima in the diagram. They are assigned O_{1A}, O_{1B}, and O_4 (fourfold degenerated) and the corresponding vectors parallel to the Si-Si bond for each of them, according to Fig. 1, are given. For a saddle point of trigonal symmetry there are two different energy barriers separating these three minima. They are assigned as T_{2A} and T_{2B} and for each of them there are two equivalent configurations of the trigonal axis. The O_4 minimum for the neutral state has been chosen as a reference point for the energy scale. From the alignment results we conclude that the neutral charge state minima O_{1A} and O_{1B} shift equally in respect to the O_4 reference point ($\alpha^0_{\langle 111 \rangle} = 0$), and from the measurements of the peak splitting we conclude that the energy differences between VO^- and VO^0 in the O_{1A} and O_4 configurations do not change significantly with the stress whereas the peak that moves with stress is the one that also increase during alignment as shown in Fig. 4. As a result, we ascribe the measured stress-increasing barrier to T_{2B} configuration.
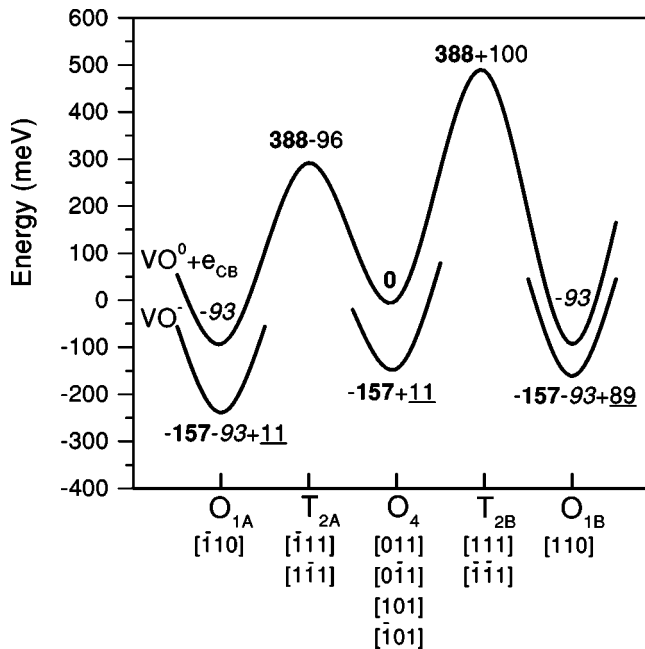
FIG. 6. The total energy diagram for the VO complex stressed along the [110] direction. Below each minimum the corresponding vectors parallel to the Si-Si bond, according to Fig. 1, are given. For the maxima the vectors indicate orientations of the trigonal axes. Numbers of the vectors are degeneracies of particular extrema. All values of energies are given referred to the energy of the O_4 point for VO^0 and have errors of few meV. The numbers in a bold font are for the zero stress, in italic are values obtained from the alignment experiments and calculated for 1 GPa, the underlined values are obtained from Laplace DLTS peak splitting. The increase of the barrier of the T_{2B} point has been measured directly, the decrease in T_{2A} is estimated.

Unfortunately, absolute shifts of the top of the barrier and the stable configuration cannot be derived from the data independently of the hydrostatic components because both of them have to be known. For the purpose of estimating the shift of the T_{2A} saddle point we assumed that the piezospectroscopic tensor of the stable configuration is traceless ($B_1^0 + B_2^0 + B_3^0 = 0$) and ascribe a hydrostatic stress component solely to the saddle point configuration. On this basis from the decrease of the reconfiguration barrier observed in the $\langle 100 \rangle$ direction we can now estimate this "relative" hydrostatic component to be $B_h = -9$ eV. Accordingly, from the observed increase of the reconfiguration barrier for the $\langle 110 \rangle$ direction we can estimate the parameter $B_t = -16$ eV and thereby obtain a value for the T_{2A} saddle energy.

The hydrostatic component of the piezospectroscopic tensor for the saddle point configuration describes the change of the defect volume of the saddle-point configuration relative to the stable configuration. Thus, the negative value of B_h means that the effective volume of the unit cell with oxygen in the saddle point position has increased compared to the structure with oxygen forming the Si-O-Si bridge. Recently, Deák has given arguments for that threefold coordinated oxygen in covalent crystals has to be positively charged.[37] In accordance with this, to keep the whole defect neutral, an effective electronic charge has to move from oxygen towards the dangling bond.

A consequence of the trigonal symmetry of the saddle point is that the barrier in the T_{2A} point decreases with stress proportionally with the $B_t s_{44}$ term. The effect of this barrier reduction can be only observed at very high stresses where it is possible to resolve the O_{1A} and O_4 configurations (see inset in Fig. 4). At these stresses instead of the expected 1:4 splitting (proportional to the number of the O_{1A} and O_4 configurations), the O_{1A} configuration has been observed with a much higher concentration than O_4 because high stress reduces the T_{2A} barrier so much that even at the measurement temperature (90 K) a partial defect alignment (from O_4 to O_{1A} configuration) occurs. This partial alignment during measurement at high stress has been confirmed by aligning at higher temperatures. As can be seen from the dashed line in the inset in Fig. 4 all centers remaining in the O_4 configuration can be converted to O_{1B}.

The VO complex diffuses via single jump events with the barrier of 2 eV.[38] From comparison of reconfiguration and diffusion rates it can be shown that at 300 °C one diffusion jump occurs per 10^{14} reorientation events. As discussed above, the saddle point configuration may result in a very strong internal electrical polarization of the complex, which may create a significant attractive force towards the vacancy which we may associate with the silicon atom not attached to oxygen. Consequently, the saddle point configuration of the complex can be a starting point for the vacancy moving to the neighboring unit cell in the event that a local vibration of the silicon atom towards the vacancy occasionally is followed by an immediate oxygen jump. This seems to be a plausible rationalization of how vacancies can drag oxygen atoms through the crystal to form larger oxygen aggregates.

*E-mail: dobacz@ifpan.edu.pl

[1] *Early Stage of Oxygen Precipitation in Silicon*, edited by R. Jones, Vol. 17 of *NATO Advance Science Institutes, Series 3: High Technology* (Kluwer Academic, Dordrecht, 1996), Vol. 17.

[2] R. C. Newman, J. Phys. C **18**, L967 (1985).

[3] L. I. Murin, T. Hallberg, V. P. Markevich, and J. L. Lindström,

Phys. Rev. Lett. **80**, 93 (1998).

[4] J. W. Corbett, G. D. Watkins, and R. S. McDonald, Phys. Rev. **135**, A1381 (1964).

[5] B. G. Svensson, J. L. Lindström, and J. W. Corbett, Appl. Phys. Lett. **47**, 841 (1985).

[6] A. S. Oates and R. C. Newman, Appl. Phys. Lett. **49**, 262 (1986).

[7] R. C. Newman, J. Phys.: Condens. Matter **12**, R335 (2000).

[8] D. H. Hwang, B. Y. Lee, H. D. Yoo, and O. J. Kwon, J. Cryst. Growth **213**, 57 (2000).

[9] B. G. Svensson and J. L. Lindström, Phys. Rev. B **34**, 8709 (1986).

[10] P. Pellegrino, P. Lévêque, J. Lalita, A. Hallén, C. Jagadish, and B. G. Svensson, Phys. Rev. B **64**, 195211 (2001).

[11] C. A. Londos, I. V. Antonova, M. Potsidou, A. Misiuk, J. Bak-Misiuk, and A. K. Gutacovskii, J. Appl. Phys. **91**, 1198 (2002).

[12] L. Dobaczewski, K. Bonde Nielsen, O. Andersen, L. Rubaldo, K. Gościński, and A. R. Peaker, in *Proceedings of the 25th International Conference on the Physics of Semiconductors*, Osaka 2000, edited by N. Miura and T. Ando (Springer, New York, 2001), p. 1427.

[13] J. C. Mikkelsen, Jr., Appl. Phys. Lett. **40**, 336 (1982).

[14] M. Ramamoorthy and S. T. Pantelides, Phys. Rev. Lett. **76**, 267 (1996).

[15] M. Needels, J. D. Joannopoulos, Y. Bar-Yam, S. T. Pantelides, and R. H. Wolfe, in *Defects in Materials*, edited by P. D. Bristone *et al.*, Mater. Res. Soc. Symp. Proc. **209** (MRS, Warrendale, 1991), p. 103.

[16] M. N. Levin and B. A. Zon, Phys. Lett. A **260**, 386 (1999).

[17] G. D. Watkins and J. W. Corbett, Phys. Rev. **121**, 1001 (1961).

[18] G. G. DeLeo, W. B. Fowler, and G. D. Watkins, Phys. Rev. B **29**, 3193 (1984).

[19] D. J. Chadi, Phys. Rev. Lett. **77**, 861 (1996).

[20] M. Pesola, J. von Boehm, T. Mattila, and R. M. Nieminen, Phys. Rev. B **60**, 11449 (1999).

[21] J. Coutinho, R. Jones, P. R. Briddon, and S. Öberg, Phys. Rev. B **62**, 10824 (2000).

[22] C. P. Ewels, R. Jones, and S. Öberg, Mater. Sci. Forum **196-198**, 1297 (1995).

[23] A. Dal Pino, M. Needels, and J. D. Joannopoulos, Phys. Rev. B **45**, 3304 (1992).

[24] A. A. Kaplyanskii, Opt. Spectrosc. **16**, 329 (1964).

[25] J. M. Meese, J. W. Farmer, and C. D. Lamp, Phys. Rev. Lett. **51**, 1286 (1983).

[26] According to the standard crystallographic notation the [110] symbol means this particular direction (see Fig. 1). While the ⟨110⟩ symbol means: a group of equivalent directions, here e.g., [$\bar{1}$10], [011], etc. The (110) symbol means: the plane perpendicular to ⟨110⟩.

[27] L. Dobaczewski, P. Kaczor, I. D. Hawkins, and A. R. Peaker, J. Appl. Phys. **76**, 194 (1994).

[28] J. F. Nye, *Physical Properties of Crystals, Their Representation by Tensor and Matrices* (Clarendon Press, Oxford, 1957).

[29] Xiu-chen Yao, Jian-xun Mou, and Guo-gang Qin, Phys. Rev. B **35**, 5734 (1987).

[30] D. V. Lang, J. Appl. Phys. **45**, 3023 (1974).

[31] Jian-xun Mou, Xiu-chen Yao, and Guo-gang Qin, Mater. Sci. Forum **10-12**, 481 (1986).

[32] G. A. Samara and C. E. Barnes, Phys. Rev. Lett. **57**, 2069 (1986); G. A. Samara, Phys. Rev. B **36**, 4841 (1987).

[33] A. Hallén, N. Keskitalo, F. Masszi, and V. Nágl, J. Appl. Phys. **79**, 3906 (1996).

[34] C. H. Henry and D. V. Lang, Phys. Rev. B **5**, 989 (1977).

[35] G. D. Watkins in Ref. 1, p. 1.

[36] A consequence of the adiabaticy of the reconfiguration process is that no trajectory hysteresis is possible and the reorienting atom follows the total energy valley. See, e.g., Ref. 14 for a more detailed discussion.

[37] P. Deák in Ref. 1, p. 163.

[38] See Fig. 10 in Ref. 7, and references therein.